ACS APPLIED MATERIALS & INTERFACES

www.acsami.org

Research Article

Novel Near-Infrared Light-Induced Triple-Shape Memory Composite Based on Poly(ethylene-*co*-vinyl alcohol) and Iron Tannate

Yongkang Bai,* Jiamei Liu, Junping Ju, and Xin Chen*

Cite This: https://doi.org/10.1021/acsami.1c05166

Read Online

ACCESS | Metrics & More | Article Recommendations | Supporting Information

ABSTRACT: Remote controllability and multiple-shape memory performance are two important functions for shape memory polymers (SMPs) in engineering applications, which are still a challenge to achieve via a facile approach. Herein, we synthesized a shape memory composite with near-infrared (NIR) light-induced triple-shape memory performance by in situ formation of iron tannate (FeTA) nanoparticles in cross-linked poly(ethylene-*co*-vinyl alcohol) (EVOH). EVOH possessed two transition temperatures enabling the composites with triple-shape memory behavior, while FeTA nanoparticles served as the photothermal conversion factor for NIR light-induced responsiveness. Because the light-induced triple-shape memory performance of the composite is highly dependent on its photothermal conversion property, the control of FeTA doping would also be an effective solution to prepare light-induced multiple-SMPs with various shape transformations. Moreover, the composites exhibited high light-driving recovery stress, which could lift burdens 1600 times heavier than their own weight, indicating their great potential as a smart soft actuator for various applications.

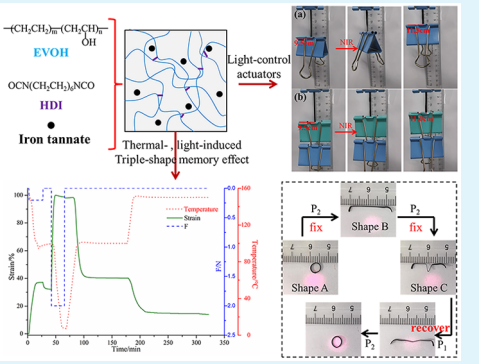

KEYWORDS: *iron tannate nanoparticles, poly(ethylene-co-vinyl alcohol), NIR responsiveness, triple-shape memory effect, light-driving actuators*

1. INTRODUCTION

Shape memory polymers (SMPs) have attracted widespread attention because of their smart changing capability, where they are able to recover from a temporary shape to a predesigned original shape upon applying external stimuli such as heat, light, electric current, solvent or pH.[1−5] Compared with other stimuli, near-infrared (NIR) light possesses many distinctive advantages, such as convenient use, remote and accurate control, and noncontact with little intervention in the surrounding environment,[6,7] which allows NIR light-induced SMPs to be applied in soft actuators, biomedical devices, microfluidic devices, and micro-electromechanical systems.[8−12]

The most common approach to achieve NIR light responsive SMPs is introducing photothermal reagents into thermal-induced SMPs, such as metal nanoparticles, carbon nanomaterials, conjugated polymers, rare earth organic complexes, and black phosphorus.[13−17] But, attributed to the poor compatibility of photothermal reagents in polymeric matrix, the direct doping strategy usually causes a dilemma in that a small amount of photothermal reagents would lead to low responsive speed and activating efficiency, while increasing the doping amount would result in the aggregation of fillers and phase segregation, consequently sacrificing the mechanical and shape memory properties. To resolve this limitation, several methods have been developed, such as chemical modification on conventional photothermal reagents and employing more compatible organic dyes.[18−20] However, either the photothermal reagents or the improvement methods usually require a complicated chemical synthesis or modification process, which will significantly increase the complexity and cost of preparation. Therefore, it is still a challenge to obtain a light-induced SMP with high NIR responsive efficiency by a simple method. Considering that the problem majorly originated from aggregation of photothermal reagents after direct doping, the in situ formation of photothermal reagents would be an effective solution. One of the facile approaches to form photothermal reagents is the reaction between ferric ions and tannic acid, a reaction observed, for example, when an apple or pear is cut with an iron knife. This reaction is able to rapidly produce iron tannate (FeTA) nanoparticles with a high photothermal conversion efficiency of about 40%,[21,22] which provides an effective way to resolve the aggregation issue via in situ generation of FeTA nanoparticles in solid polymer matrix.

In addition to stimuli-responsiveness, multiple-shape memory performance is also important to SMPs, which allows devices to realize complicated shape changes and accurate

Received: March 19, 2021
Accepted: April 27, 2021

Scheme 1. Preparation Route of EVOH/FeTA Composites

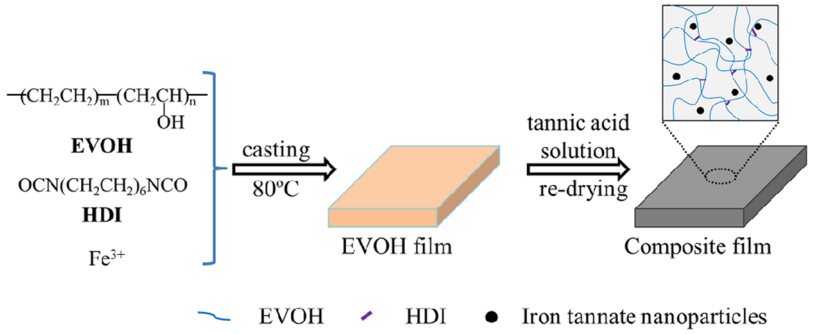

activating behaviors. Therefore, developing novel triple-shape memory polymers (triple-SMPs) to upgrade the traditional dual-SMPs has received more and more attention.[23−25] Although some studies involved the fabrication of triple-SMPs, the triple-shape memory property mainly relied on introducing two separated thermal transitions (glass transition temperature or melting point) into one polymer network, which was achieved by copolymerization, blending, or interpenetrating polymer networks.[26−29] These methods usually need complicated molecular design and synthesis processes, which significantly hindered their applications. Moreover, these studies mainly concentrate on thermal-induced triple-SMPs; light-induced triple-SMPs are rarely reported.

In this study, a commercial copolymer, poly(ethylene-*co*-vinyl alcohol) (EVOH), was adopted as the matrix to fabricate NIR light-induced triple-shape memory composites via a facile two-step method utilizing its intrinsic existence of two separated transitions (polyethylene and poly(vinyl alcohol)).[30] First, EVOH in dimethylformamide containing ferric ions was cross-linked by hexamethylene diisocyanate to realize the shape memory performance. After that, the NIR light responsiveness of composites was achieved by simply immersing the cross-linked EVOH films into tannic acid solution to form FeTA nanoparticles. By this method, the FeTA nanoparticles could be dispersed into the composites homogeneously, further endowing the composites with the excellent mechanical property. Based on the great photothermal property of FeTA nanoparticles and dual transition temperatures of EVOH, the composites showed excellent light-induced triple-shape memory effects, which would make them a promising candidate for application in soft actuators.

2. EXPERIMENTAL SECTION

2.1. Materials. Poly(ethylene-*co*-vinyl alcohol) (EVOH) (ethylene content 27 mol %, M_n = ~4 × 10^4 g mol^{-1}) was purchased from Shanghai ZZBIO CO., Ltd. Hexamethylene diisocyanate (HDI) was received from Aladdin Industrial Corporation. Tannic acid (TA) and anhydrous ferric chloride ($FeCl_3$) were supplied by Shanghai Mcaklin Biochemical Co., Ltd. *N*,*N*′-Dimethylformamide (DMF), isopropanol, and other reagents were bought from Tianjin Chemical Reagents Company.

2.2. Preparation of Shape Memory Composites. The shape memory EVOH composite was prepared by a two-step method. First, the shape memory property of EVOH was achieved by using HDI as the chemical cross-linking reagent. The amount of 2 g of EVOH and a certain amount of anhydrous $FeCl_3$ (0−0.1 g) were dissolved in 30 mL of DMF after stirring at 90 °C, and 0.2 g of HDI was added to the solution after being cooled down to room temperature. Next, the mixture was cast onto a glass plate and further reacted at 80 °C for 12 h to afford cross-linked EVOH, which was named as EHFe*x* (where *x* represents the weight percent of $FeCl_3$ to EVOH). Second, the NIR light responsiveness was achieved by simply immersing the prepared EHFe*x* in 0.02 g mL^{-1} tannic acid (TA) aqueous solution for 24 h to form FeTA nanoparticles in the composite. Then the composite films were washed with water five times and re-dried at room conditions (room temperature about 20 °C and relative humidity about 35%) for 5 days. The dried composite films were collected for further investigation and named as EHFe*x*D (unless otherwise indicated).

2.3. Characterization. The cross-linked reaction was confirmed by Fourier transform infrared (FTIR) spectroscopy performed with a Nicolet iS50 IR spectrophotometer (America). Gel content (G) was measured to evaluate the cross-linked reaction of composites according to $G = m_s/m_0 \times 100\%$ by Soxhlet extraction. Here, m_0 is the original weight of the samples and m_s is the dried weight of the samples after Soxhlet extraction with an isopropanol/water solution (3:1 at volume) for 48 h. The microstructure of the fracture surface was investigated by scanning electron microscopy (SEM; TESCAN MALA3 LMH, Czech Republic). The thermal properties of composites were investigated by dynamical mechanical analysis (DMA; DMA242E, NETZSCH, Germany) and differential scanning calorimetry (DSC; DISCOVER DSC250, America). For DMA tests, the samples with dimensions of about 20 × 3 × 0.3 mm^3 were heated from 10 to 200 °C at a rate of 5 °C min^{-1}. For DSC, the samples were heated from 20 to 150 °C and equilibrated for 5 min to eliminate the thermal history. Then the samples were cooled to 20 °C and reheated to 200 °C, and the heating rate of the whole process was 10 °C min^{-1}. The dual transition temperature of composites was confirmed by the second heating curves. The mechanical property of composites was measured by a universal testing machine (WANCE ETM 103B-TS, China) under a uniaxial tension mode with a stretching speed of 10 mm min^{-1}. All specimens were cut to a dog bone shape according to ISO527-2/1BB, and each sample was tested at least five times.

2.4. Shape Memory Property of Composites. The shape memory performance was confirmed by DMA through a TMA mode, and details were as follows: (1) a film sample (20 × 3 × 0.3 mm^3) was stretched under a constant stress at 100 or 150 °C to reach a max strain of ε_A; (2) the sample was cooled to 10 °C, and the external stress was removed to afford a temporary strain ε_A; (3) the sample was reheated to 100 or 150 °C to recover its original shape (ε_C). Then shape fixity ratio (R_f) and shape recovery ratio (R_r) were adopted to evaluate the shape memory performance according to formulas 1 and 2.[31] The recovery stress was measured at an isostrain mode by DMA: a composite film was heated from 20 to 200 °C with a strain of 120% at a heating rate of 5 °C min^{-1}.

$$R_f = \varepsilon_B/\varepsilon_A \times 100\% \quad (1)$$

$$R_r = (\varepsilon_B - \varepsilon_C)/\varepsilon_B \times 100\% \quad (2)$$

The photothermal conversion performance was investigated by using a thermal imaging camera (FLIR ONE PRO, FLIR, USA) under irradiation of NIR light (808 nm), and at least five samples were tested. Then NIR light-induced shape memory property was investigated by performing a tensile-cycle test, and at least three

https://doi.org/10.1021/acsami.1c05166
ACS Appl. Mater. Interfaces XXXX, XXX, XXX−XXX

samples were tested: (1) a sample (20 × 3 × 0.3 mm^3) was stretched to a strain of ε_A after heating to 100 °C by NIR light irradiation; (2) the sample was cooled to room temperature and the external load was removed to obtain a temporary strain (ε_B); (3)finally, the sample was reheated to 100 °C by NIR light irradiation again to recall the original shape (ε_C). The light-induced R_r and R_f were also calculated according to formulas 1 and 2.

3. RESULTS AND DISCUSSION

In this study, a NIR light-induced shape memory composite based on EVOH was prepared by a two-step method as presented in Scheme 1. First, the shape memory performance was achieved by cross-linking EVOH with HDI and the cross-linked reaction was confirmed by FTIR spectra. As shown in Figure 1, the characteristic peak of −OH shifted from 3285

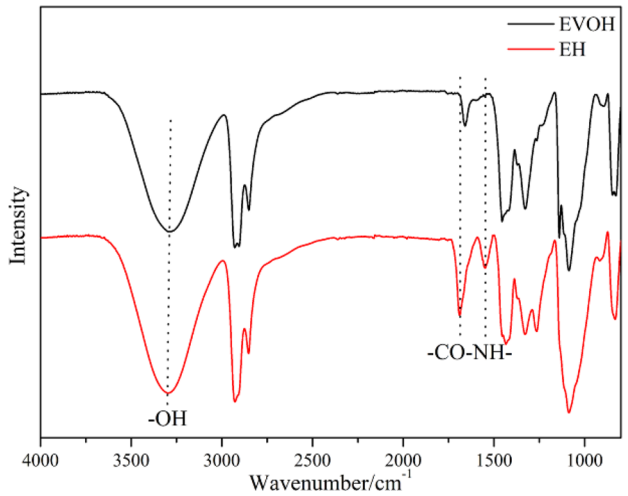

Figure 1. FTIR spectra of EVOH and cross-linked EH.

cm^{-1} of EVOH to 3299 cm^{-1} of EH due to the consumption of −OH by HDI. In addition, the appearance of peaks at 1689 and 1548 cm^{-1} on the spectrum of EH was attributed to the characteristic peaks of −CO−NH−, which confirmed the successful reaction between EVOH and HDI.[32] Then the cross-linked reaction was further evaluated with the gel content of composites, which was carried out by Soxhlet extraction tests. All the composites showed a high gel content of over 95%, validating the formation of a cross-linked network structure.

Next, the NIR light responsiveness of composites was realized by in situ formation of FeTA nanoparticles as photothermal conversion reagents. Through a simple soaking process in TA solution, the irregular FeTA nanoparticles formed in the polymer network and their particle size was determined to be about 150 nm (confirmed by SEM images in Figure S1), which was similar to previous study.[22] Then the dispersion state of FeTA nanoparticles was investigated by SEM analysis of the micromorphology of EVOH and its composites. In addition, a control sample with a similar TA content of EHFe5D was prepared by directly adding TA to the EVOH solution before the curing process. The TA content of about 1.9 wt % EHFe5D was calculated according to the weight change after the formation of FeTA nanoparticles. As shown in Figure 2, pure EVOH showed a smooth fracture surface, while the introduction of cross-linked interaction increased the roughness due to the enhancement of the material's toughness. Then the roughness was further increased

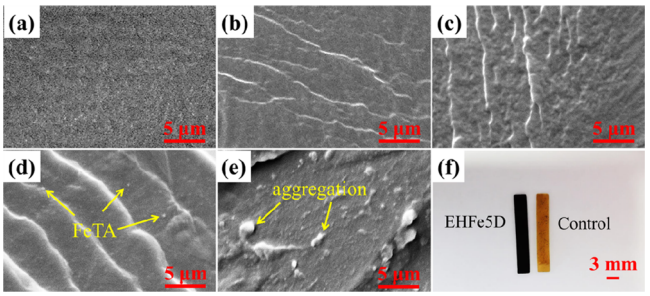

Figure 2. SEM images of the fracture of (a) EVOH, (b) EH, (c) EHFe5, (d) EHFe5D, and (e) control sample. (f) optical images of EHFe5D and control sample.

by the introduction of $FeCl_3$ or FeTA attributed to the increase of energy dissipation brought about by fillers during the fracturing process.[33,34] As observed from the fracture surface of EHFe5D in Figure 2d, the uniform dispersion of FeTA nanoparticles could be confirmed by the distribution of the dots (as indicated by arrows in the images). But for the control sample presented in Figure 2e, many aggregations could be observed clearly on the fracture surface due to the low compatibility of FeTA nanoparticles. This difference could be seen more obviously in their macro images in Figure 2f: EHFe5D presented a uniform black color, while the control sample showed obvious aggregations.

The mechanical property is important for the application of shape memory materials, which are affected greatly by the chemical structure and dispersion state of fillers. Here the mechanical property of composites was investigated by using a tensile machine, and the results are presented in Figure 3 and

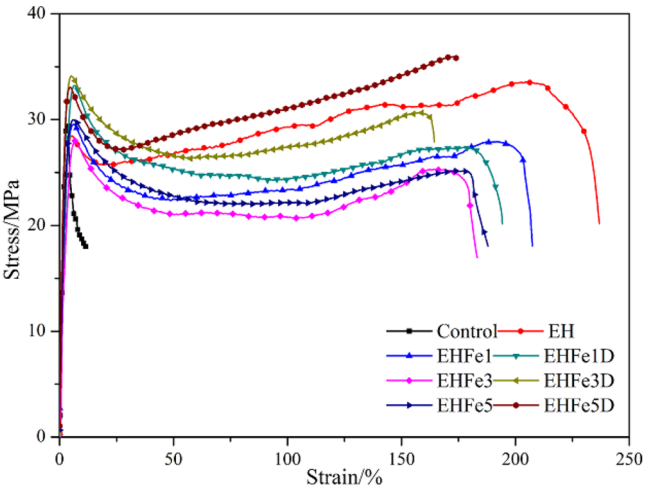

Figure 3. Stress−strain curves of EH and composites.

Table 1. Although the original EVOH was brittle, the cross-linked EH showed high toughness after the introduction of cross-linked networks, and its elongation at break (ε) and tensile strength (σ) could reach about 238.9% and 34.1 MPa, respectively. After being doped with $FeCl_3$, the elongation at break and tensile strength of EHFe*x* were reduced to 186% and 28.4 MPa, respectively, due to the incompatibility of $FeCl_3$. Then the formation of FeTA nanoparticles could enhance the tensile strength of composites to 33.8 MPa due to the reinforcement of nanoparticles. Compared with EH, although the elongation at break of the composites was

https://doi.org/10.1021/acsami.1c05166
ACS Appl. Mater. Interfaces XXXX, XXX, XXX−XXX

Table 1. Mechanical, Thermal, and Light-Induced Shape Memory Properties of EH and Its Composites

sample	σ (MPa)	ε (%)	T_g (°C)	R_f	R_r
EH	34.1 ± 0.7	238.9 ± 3.0	56.7		
EHFe1	31.2 ± 2.3	204.0 ± 5.0	73.1	98.6 ± 0.5	99.6 ± 0.3
EHFe3	28.4 ± 0.6	186.4 ± 4.4	72.6	98.3 ± 0.6	99.7 ± 0.1
EHFe5	29.3 ± 0.8	187.4 ± 0.9	72.8	98.4 ± 0.4	99.0 ± 0.9
EHFe1D	32.8 ± 0.5	201.0 ± 9.6	74.3	97.3 ± 0.4	98.1 ± 0.6
EHFe3D	33.0 ± 0.8	171.7 ± 2.1	74.1	97.1 ± 0.7	98.2 ± 0.5
EHFe5D	33.8 ± 0.5	177.8 ± 5.1	73.7	97.3 ± 0.9	98.1 ± 0.6

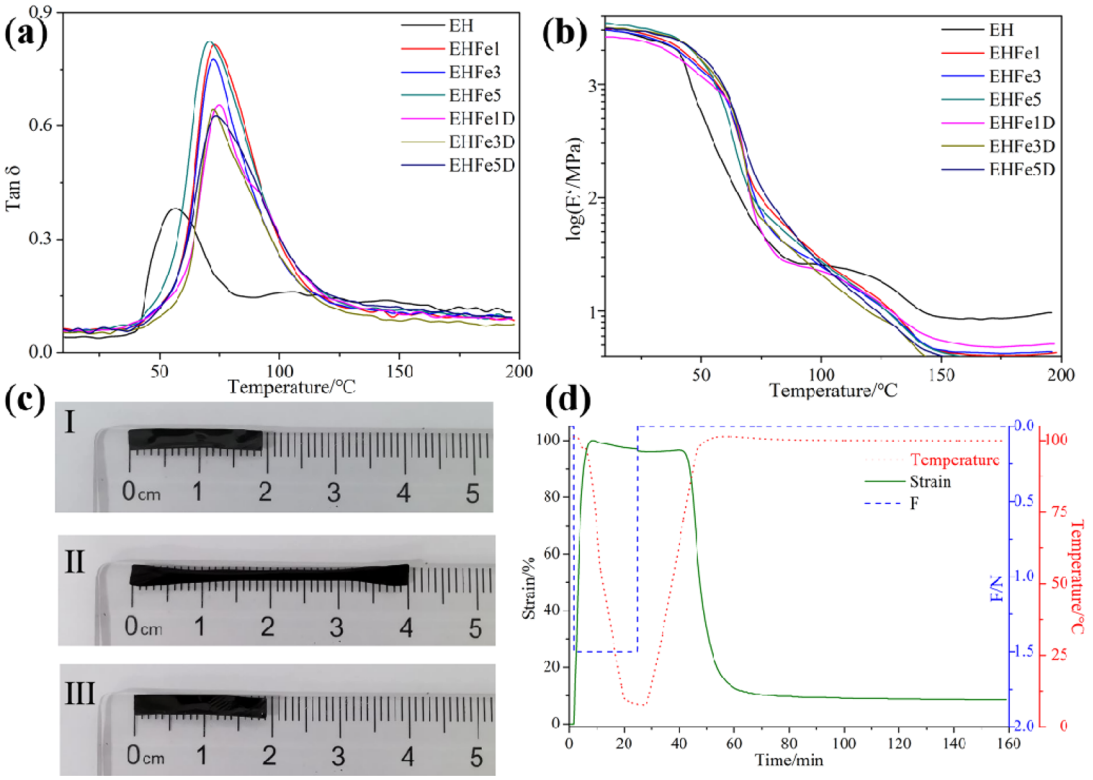

Figure 4. (a) Loss factor (tan δ) curves and (b) storage modulus (E') curves of EH and composites; (c) thermal-induced shape memory process of EHFe1D; (d) shape memory cycle curves of EHFe1D carried out by DMA.

reduced to about 170%, the composites were still strong enough to realize shape memory performance. Moreover, the control sample was also tested and it was quite brittle with an elongation at break of about 10% due to its serious aggregations. The results demonstrated that the introduction of FeTA nanoparticles by in situ synthesis was indeed beneficial to the uniform distribution of nanoparticles and the mechanical property of composites.

Prior to the investigation of the shape memory performance, the switching temperature of composites was confirmed by DMA. As shown in Figure 4a and Table 1, the glass transition temperature of EH was about 56.7 °C, while it increased to about 73 °C with the doping of $FeCl_3$ and then increased slightly to about 74 °C after the formation of FeTA nanoparticles, which may be attributed to the resistance effect of fillers on polymer chains.[35] This phenomenon was further analyzed by the storage modulus curves in Figure 4b, and the results showed that two rubbery plateaus around 100 and 145 °C appeared on the curves, especially EH and EHFe1D, demonstrating the existence of two separated transition temperatures. These two transition temperatures belonged to the T_g of PVA chains and T_m of polyethylene chains, which could be further confirmed by DSC curves in Figure S2. These results suggested that the composites may realize not only dual-shape memory performance but also triple-shape memory performance.

The dual-shape memory property of composites was first investigated by a manual tensile-cycle process, which is shown in Figures 4c and S3 and in Video S1. During the shape memory cycle process, the sample was stretched to a strain of about 100% at 100 °C and cooled to room temperature to fix the temporary shape, and then the deformed sample was reheated to 100 °C to recall the original shape. It can be clearly observed that all the composites could show an excellent shape memory property with a shape fixity ratio (R_f) and shape recovery ratio (R_r) of over 98% and 99%, respectively. Furthermore, the shape memory property of the composite was quantified by DMA, and a typical cycle process of EHFe1D with 100 °C as the programming temperature is presented in Figure 4d. It also could be found that the composite exhibited a high shape memory performance with R_f and R_r of about 98.6% and 91.5%, respectively. The reduction of R_r calculated by DMA was attributed to the minimum detection limitation of the instrument. Nonetheless, the results

https://doi.org/10.1021/acsami.1c05166
ACS Appl. Mater. Interfaces XXXX, XXX, XXX−XXX

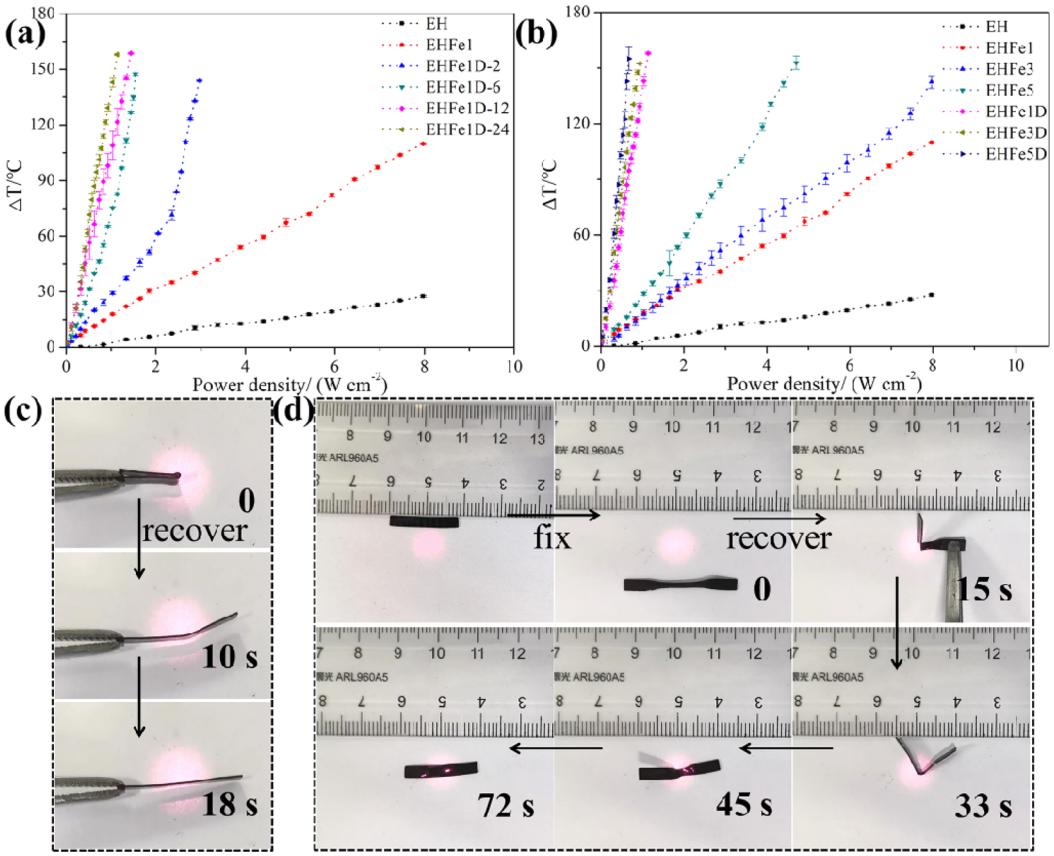

Figure 5. (a) Photothermal conversion efficiency of EHFe1D-*x*; (b) Photothermal conversion efficiency of EH and composites; (c,d) NIR light-induced shape memory behavior of EHFe1D.

demonstrated that the cross-linked EVOH was able to exhibit an outstanding thermal-induced shape memory property.

To confirm the NIR light responsiveness, an infrared thermal imager was used to investigate the photothermal conversion effect of the composites under 808 nm NIR light irradiation. The maximum temperatures under different power density of NIR light were recorded. Here, EHFe1 with different immersion times, named as EHFe1D-*x* (where *x* represents reacting hours), was measured to investigate the effect of reacting time in TA solution on the photothermal conversion performance, and the thermal images of EHFe1D-24 are presented as examples in Figure S4. It was obvious that the temperature increased rapidly with the increase of power density, and it could reach 150 °C under only 0.93 W cm^{-2} of NIR light irradiation, indicating the high photothermal conversion efficiency of FeTA nanoparticles. Figure 5a demonstrates that the gradient of curves increased quickly with the increase of reacting time to 12 h and then increased slightly when approaching 24 h. It indicated that the degree of reaction had been close to saturation when the reacting time approached 24 h, which was also the reason why 24 h was determined to prepare all EHFe*x*D composites. Then the photothermal conversion performance of all composites was investigated, and the results are shown in Figure 5b. Extracting from the variation of curves, the photothermal conversion efficiency of composites increased rapidly with the increase of $FeCl_3$ or FeTA nanoparticles, and the photothermal conversion efficiency of EHFexD was much higher than that of EHFex. All these results demonstrated that the composites indeed could exhibit excellent NIR light responsiveness with the introduction of FeTA nanoparticles.

Then the NIR light-induced shape memory performance of EHFe*x*D was investigated by a bending-recovery test and a tensile-cycle test under irradiation of 808 nm NIR light, and EHFe1D was taken as an example in Figure 5c,d and Video S2. As shown in Figure 5c, a straight sample was folded in half after heating to 100 °C by 0.57 W cm^{-2} of NIR light irradiation (obtained from the curve of Figure 5a), and the temporary shape was fixed by equilibrating it at room temperature. Then the deformed sample was exposed to NIR light again to recover its original shape, and the light-induced shape recovery process was recorded with a digital camera. The results clearly showed that the original straight shape of the sample could be recovered completely within merely 18 s. For the tensile-cycle test in Figure 5d, the sample was stretched to a strain of about 50% under NIR light irradiation and the rest of the process was similar to the bending-recovery test. It was also clearly observed that the original shape of EHFe1D could be fully recalled by NIR stimulus within 72 s. The extension of recovery time was attributed to its larger deformation. In addition, the light-induced shape memory property of composites was quantitatively evaluated by R_f and R_r. As presented in Table 1, all the composites exhibited a high light-induced shape memory property with R_f and R_r both being over 97%.

According to the results of the thermal properties, the composites possessed two transition processes, the glass transition of PVA and melting process of PE, which were the structural basis of triple-shape memory behavior. Therefore,

https://doi.org/10.1021/acsami.1c05166
ACS Appl. Mater. Interfaces XXXX, XXX, XXX−XXX

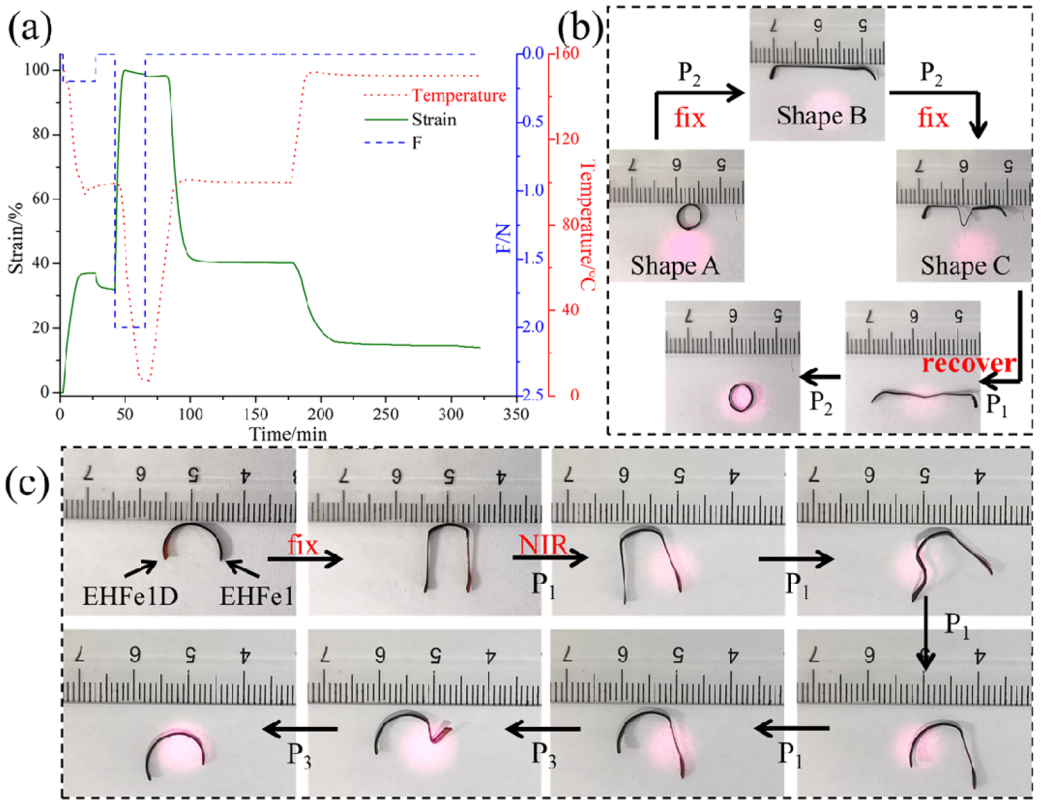

Figure 6. (a) Thermal-induced shape memory cycle curve of EHFe1D; (b) light-induced triple-shape memory behavior EHFe1D; (c) light-induced triple-shape memory behavior of composite with partial doping of FeTA nanoparticles. (Here, P_1 = 0.57 W cm^{-2}, P_2 = 0.93 W cm^{-2}, and P_3 = 5.90 W cm^{-2}.)

EHFe1D was chosen as an example again to investigate the triple-shape memory performance. First, the thermal-induced triple-shape memory performance was carried out by DMA. As shown in Figure 6a, the original film sample (ε_A) was heated up to 150 °C, which is above the T_m (145 °C), and stretched to a temporary shape B ($\varepsilon_{b,load}$) under an external load. Then the sample was cooled to 100 °C, a temperature between T_m and T_g, and the external load was removed to fix the temporary shape B (ε_b). The sample was further stretched to a second temporary shape C ($\varepsilon_{C,load}$) under a higher load then was cooled to 10 °C (below the T_g of 75 °C), and the load was removed to fix shape C (ε_C). The shape fixity ratio of each shape was calculated using formula 3. In the subsequent recovery step, the sample was reheated and equilibrated at 100 and 150 °C to recall the shape B ($\varepsilon_{B,rec}$) and original shape A ($\varepsilon_{A,rec}$) step by step. The shape recovery ratios $R_{r(C\to B)}$ and $R_{r(B\to A)}$ were calculated according to formula 4.[36]

$$R_{f,X\to Y} = (\varepsilon_Y - \varepsilon_X)/(\varepsilon_{Y,load} - \varepsilon_X) \quad (3)$$

$$R_{r,Y\to X} = (\varepsilon_Y - \varepsilon_{X,rec})/(\varepsilon_Y - \varepsilon_X) \quad (4)$$

Extracting the data from the curve in Figure 6a, the shape fixity of shape B ($R_{f,\,A\to B)}$) in the first fixing step was about 86.2% while it was 98.8% for shape C. The reason for the lower shape fixity of shape B was attributed to the two reversible phases (PE and PVA chains) being stretched during deforming process but only the strain resulting from PE chains could be stored at 100 °C after the removal of the external load. During the following recovery process, the shape recovery ratios of shape B ($R_{r,\,C\to B}$) and shape A ($R_{r,\,B\to A}$) were about 87.8% and 81.6%, respectively. Because the cross-linked reaction could only occur between PVA chains, the PE chains still retained the un-cross-linked structure, leading to the low value of $R_{r,\,B\to A}$. This phenomenon could be also confirmed by the dual-shape memory process with 150 °C as the programming temperature (Figure S5), during which the shape recovery ratio was only about 85.2%, accompanying the addition of the PE phase as the reversible phase. Thus, the composite indeed could exhibit the triple-shape memory property based on PVA and PE chains as reversible phases.

It has been confirmed that the composites could reach different temperatures by adjusting the power density of the NIR light, so the light-induced triple-shape memory behavior could also be easily realized. The composite EHFe1D was taken as an example, and the results are presented in Figure 6b and Video S3. Similar to the thermal-induced triple-shape memory process, the original sample with a circle shape was stretched to shape B under 0.93 W cm^{-2} of NIR light (corresponding to 150 °C) and fixed at room temperature. Then it was deformed to shape C under 0.57 of W cm^{-2} NIR light (corresponding to 100 °C) and fixed at room temperature again. During the recovery steps, the deformed sample could recover to shape C first under 0.57 W cm^{-2} of NIR light, but then showed no shape change with the extension of irradiation time. Upon raising the power density to 0.93 W cm^{-2}, the original circle shape of the sample could be fully recovered, demonstrating that the composite was indeed able to exhibit the light-induced triple-shape memory effect.

During the investigation of light responsiveness, it was found that the photothermal conversion efficiency can be adjusted by the content of FeTA nanoparticles. For example, 5.9 W cm^{-2} of NIR light was required to activate EHFe1 to 100 °C while

https://doi.org/10.1021/acsami.1c05166
ACS Appl. Mater. Interfaces XXXX, XXX, XXX−XXX

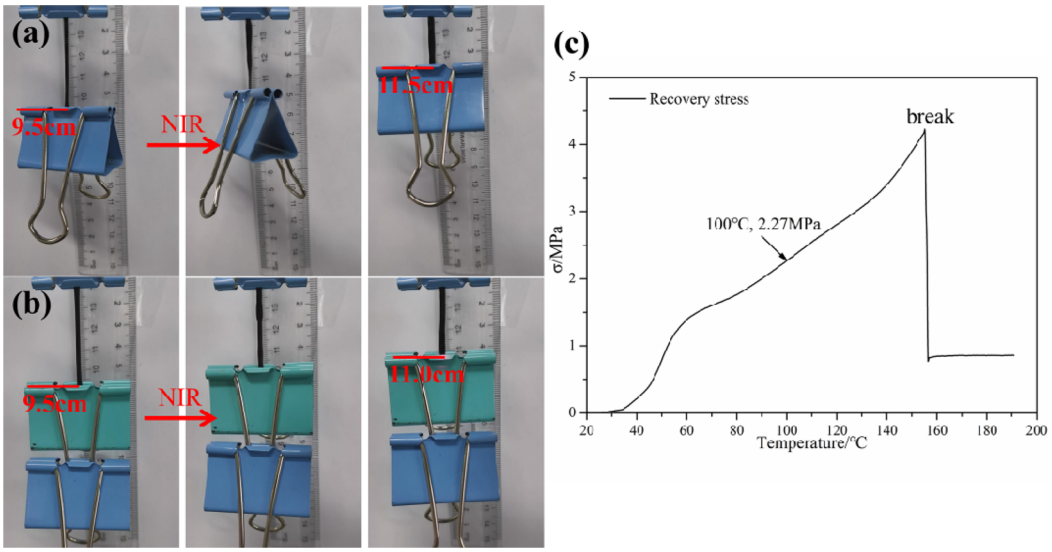

Figure 7. Light-induced driving performance of EHFe1D under (a) 16.4 g and (b) 32.8 g. (c) Recovery stress−temperature curve of EHFe1D at 120% strain.

only 0.57 W cm^{-2} was needed for EHFe1D. Therefore, another type of light-induced triple-shape memory behavior was investigated by partial introduction of FeTA nanoparticles. As shown in Figure 6c, a sample with two parts (EHFe1 and EHFe1D) was constructed through partial immersion of the EHFe1 sample into a TA solution for 24 h. The original arc shape was stretched at 100 °C and cooled to room temperature to fix the temporary shape. When exposed to 0.57 W cm^{-2} NIR light, it was observed that only the left part (EHFe1D) was able to fully recover, while no shape change was detected on the right part (EHFe1). It was because the temperature of EHFe1 only reached about 31 °C under irradiation of 0.57 W cm^{-2} NIR light. Then upon increasing the power density to 5.9 W cm^{-2}, the original shape of the right part was also recovered quickly, demonstrating that the light-induced triple-shape memory effect could be also realized by controlling the FeTA nanoparticle content in composites.

The results presented so far have revealed that the composites exhibited an outstanding NIR light-induced shape memory property and mechanical strength, indicating their application potential as light control actuators. In Figure 7, the samples (EHFe1D), with original dimensions of 20 × 3 × 0.3 mm^3 and weight of about 0.02 g, were stretched to a strain of 120% before the investigation of light-induced driving performance. As presented in Figure 7a, under irradiation of 0.57 W cm^{-2} NIR light, the sample was able to lift a burden of about 16.4 g by 2 cm, which was about 820 times heavier than the sample's weight. Bearing the limitation of burden, R_r of the sample could still reach about 80%. With the increase of burden to 32.8 g, 1640 times heavier than sample's weight, Figure 7b shows that the sample could still lift the burden up by 1.5 cm, indicating its high heavy-lift capability driven by the light-induced recovery stress. In addition, the recovery stress of EHFe1D with 120% strain was quantified by DMA at an isostrain mode. As presented in Figure 7c, the recovery stress of EHFe1D increased quickly with the increase of temperature and it reached about 2.27 MPa at 100 °C and 4.22 MPa at 150 °C. The curve also showed that the sample was broken at around 155 °C due to the reduction of the mechanical property at elevated temperature.

4. CONCLUSION

In summary, a NIR light-induced shape memory composite was fabricated by in situ synthesis of FeTA nanoparticles in cross-linked EVOH in the form of solid state. By this method, the FeTA nanoparticles could be dispersed into the EVOH matrix uniformly, endowing the composites with high mechanical strength and photothermal conversion performance. Combining the cross-linked structure linked by HDI, the EVOH composites could show excellent light-induced shape memory performance with R_f and R_r values over 97% and 98%, respectively. In addition, based on the two separated transition processes of EVOH (the glass transition of PVA and melting process of PE), the composites were able to exhibit thermal- and light-induced triple-shape memory properties. Utilizing the difference of photothermal conversion efficiency brought about by doping content, the light-induced triple-shape memory behavior also can be realized by partially doping the FeTA nanoparticles into composites, which could further widen the design strategies of NIR light-driving multishape memory polymers. Moreover, the composites exhibited high light-driving recovery stress and were able to lift a burden of weight of over 1600 times greater than the samples' weights. These superior mechanical and light-induced triple-shape memory properties will enable the application of these EVOH composites, especially in soft actuators.

■ ASSOCIATED CONTENT

Supporting Information

The Supporting Information is available free of charge at https://pubs.acs.org/doi/10.1021/acsami.1c05166.

Additional SEM image of EHFe 5d; DSC curve of EHFe1D; thermal-induced shape memory process of EHFe1D; thermal images of EHFe1D; shape memory curve of EHFe1D (PDF)

Shape memory process of EHFe1 (AVI)

NIR light-induced shape memory behavior of EHFe1D (AVI)

light-induced triple-shape memory behavior EHFe1D (AVI)

https://doi.org/10.1021/acsami.1c05166
ACS Appl. Mater. Interfaces XXXX, XXX, XXX−XXX

AUTHOR INFORMATION

Corresponding Authors

Yongkang Bai − *School of Chemical Engineering and Technology, Shaanxi Key Laboratory of Energy Chemical Process Intensification, Institute of Polymer Science in Chemical Engineering, Xi'an Jiaotong University, Xi'an, Shaanxi 710049, PR China;* orcid.org/0000-0003-3541-9349; Email: Yongkangbai@sina.com

Xin Chen − *School of Chemical Engineering and Technology, Shaanxi Key Laboratory of Energy Chemical Process Intensification, Institute of Polymer Science in Chemical Engineering, Xi'an Jiaotong University, Xi'an, Shaanxi 710049, PR China;* orcid.org/0000-0002-1224-0285; Email: Chenx2015@xjtu.edu.cn

Authors

Jiamei Liu − *Instrument Analysis Center, Xi'an Jiaotong University, Xi'an,, Shaanxi 710049, PR China*

Junping Ju − *State Key Laboratory of Bio-Fibers and Eco-Textiles, School of Materials Science and Engineering, Qingdao University, Qingdao 266000, PR China*

Complete contact information is available at: https://pubs.acs.org/10.1021/acsami.1c05166

Notes

The authors declare no competing financial interest.

ACKNOWLEDGMENTS

This work was supported by the National Natural Science Foundation of China (51903204), the "Young Talent Support Plan" of Xi'an Jiao Tong University (X.C.), the Open Project Program of State Key Laboratory of Bio-Fibers and Eco-Textiles (Y.K.B.), the Technology Foundation for Selected Overseas Chinese Scholar of Shaanxi Province (X.C.), the One Hundred Talents Program of Shaanxi Province (X.C.), the Innovation Capability Support Program of Shaanxi (No. 2018PT-28, 2019PT-05).

REFERENCES

(1) Hornat, C. C.; Urban, M. W. Shape Memory Effects in Self-Healing Polymers. *Prog. Polym. Sci.* **2020**, *102*, 101208−101223.

(2) Wu, S.; Li, W.; Sun, Y.; Pang, X.; Zhang, X.; Zhuang, J.; Zhang, H.; Hu, C.; Lei, B.; Liu, Y. Facile Fabrication of a CD/PVA Composite Polymer to Access Light-Responsive Shape-Memory Effects. *J. Mater. Chem. C* **2020**, *8* (26), 8935−8941.

(3) Lendlein, A.; Gould, O. E. C. Reprogrammable Recovery and Actuation Behaviour of Shape-Memory Polymers. *Nature Reviews Materials* **2019**, *4* (2), 116−133.

(4) Xie, H.; Yang, K.-K.; Wang, Y.-Z. Photo-Cross-Linking: A Powerful and Versatile Strategy to Develop Shape-Memory Polymers. *Prog. Polym. Sci.* **2019**, *95*, 32−64.

(5) Kirillova, A.; Ionov, L. Shape-Changing Polymers for Biomedical Applications. *J. Mater. Chem. B* **2019**, *7*, 1597−1624.

(6) Yang, Y.; Pei, Z.; Li, Z.; Wei, Y.; Ji, Y. Making and Remaking Dynamic 3D Structures by Shining Light on Flat Liquid Crystalline Vitrimer Films without a Mold. *J. Am. Chem. Soc.* **2016**, *138* (7), 2118−2121.

(7) Liu, L.; Liu, M.; Deng, L.; Lin, B.; Yang, H. Near-Infrared Chromophore Functionalized Soft Actuator with Ultrafast Photo-responsive Speed and Superior Mechanical Property. *J. Am. Chem. Soc.* **2017**, *139* (33), 11333−11336.

(8) Aksoy, B.; Besse, N.; Boom, R. J.; Hoogenberg, B. J.; Blom, M.; Shea, H. Latchable Microfluidic Valve Arrays Based on Shape Memory Polymer Actuators. *Lab Chip* **2019**, *19* (4), 608−617.

(9) Yu, L.; Yu, H. Light-Powered Tumbler Movement of Graphene Oxide/Polymer Nanocomposites. *ACS Appl. Mater. Interfaces* **2015**, *7* (6), 3834−3839.

(10) Lu, H.; Yao, Y.; Huang, W. M.; Leng, J.; Hui, D. Significantly Improving Infrared Light-Induced Shape Recovery Behavior of Shape Memory Polymeric Nanocomposite via a Synergistic Effect of Carbon Nanotube and Boron Nitride. *Composites, Part B* **2014**, *62*, 256−261.

(11) Pei, Z.; Yang, Y.; Chen, Q.; Terentjev, E. M.; Wei, Y.; Ji, Y. Mouldable Liquid-Crystalline Elastomer Actuators with Exchangeable Covalent Bonds. *Nat. Mater.* **2014**, *13* (1), 36−41.

(12) Han, D.; Morde, R. S.; Mariani, S.; La Mattina, A. A.; Vignali, E.; Yang, C.; Barillaro, G.; Lee, H. 4D Printing of a Bioinspired Microneedle Array with Backward-Facing Barbs for Enhanced Tissue Adhesion. *Adv. Funct. Mater.* **2020**, *30* (11), 1909197−1909208.

(13) Huang, J.; Fan, J.; Yin, S.; Chen, Y. Design of Remotely, Locally Triggered Shape-Memory Materials Based on Bicontinuous Polylactide/Epoxidized Natural Rubber Thermoplastic Vulcanizates via Regulating the Distribution of Ferroferric Oxide. *Compos. Sci. Technol.* **2019**, *182*, 107732−107741.

(14) Xie, H.; Li, L.; Cheng, C. Y.; Yang, K.-K.; Wang, Y.-Z. Poly(ethylene-co-vinyl acetate)/Graphene Shape-Memory Actuator with a Cyclic Thermal/Light Dual-Sensitive Capacity. *Compos. Sci. Technol.* **2019**, *173*, 41−46.

(15) Tong, L.; Liao, Q.; Zhao, Y.; Huang, H.; Gao, A.; Zhang, W.; Gao, X.; Wei, W.; Guan, M.; Chu, P. K.; Wang, H. Near-Infrared Light Control of Bone Regeneration with Biodegradable Photothermal Osteoimplant. *Biomaterials* **2019**, *193*, 1−11.

(16) Fang, L.; Chen, S.; Fang, T.; Fang, J.; Lu, C.; Xu, Z. Shape-Memory Polymer Composites Selectively Triggered by Near-Infrared Light of Two Certain Wavelengths and Their Applications at Macro-/Microscale. *Compos. Sci. Technol.* **2017**, *138* (Supplement C), 106−116.

(17) Zhou, L.; Liu, Q.; Lv, X.; Gao, L.; Fang, S.; Yu, H. Photoinduced Triple Shape Memory Polyurethane Enabled by Doping with Azobenzene and GO. *J. Mater. Chem. C* **2016**, *4* (42), 9993−9997.

(18) Ji, S.; Fan, F.; Sun, C.; Yu, Y.; Xu, H. Visible Light-Induced Plasticity of Shape Memory Polymers. *ACS Appl. Mater. Interfaces* **2017**, *9* (38), 33169−33175.

(19) Li, T.; Li, Y.; Wang, X.; Li, X.; Sun, J. Thermally and Near-Infrared Light-Induced Shape Memory Polymers Capable of Healing Mechanical Damage and Fatigued Shape Memory Function. *ACS Appl. Mater. Interfaces* **2019**, *11* (9), 9470−9477.

(20) Li, M.; Fu, S.; Basta, A. H. Light-Induced Shape-Memory Polyurethane Composite Film Containing Copper Sulfide Nanoparticles and Modified Cellulose Nanocrystals. *Carbohydr. Polym.* **2020**, *230*, 115676−115683.

(21) Liu, T.; Liu, W.; Zhang, M.; Yu, W.; Gao, F.; Li, C.; Wang, S.; Feng, J.; Zhang, X. Ferrous-Supply-Regeneration Nanoengineering for Cancer-Cell-Specific Ferroptosis in Combination with Imaging-Guided Photodynamic Therapy. *ACS Nano* **2018**, *12* (12), 12181−12192.

(22) Liu, T.; Zhang, M.; Liu, W.; Zeng, X.; Song, X.; Yang, X.; Zhang, X.; Feng, J. Metal Ion/Tannic Acid Assembly as a Versatile Photothermal Platform in Engineering Multimodal Nanotheranostics for Advanced Applications. *ACS Nano* **2018**, *12* (4), 3917−3927.

(23) Li, M.; Guan, Q.; Dingemans, T. J. High-Temperature Shape Memory Behavior of Semicrystalline Polyamide Thermosets. *ACS Appl. Mater. Interfaces* **2018**, *10* (22), 19106−19115.

(24) Tian, M.; Gao, W.; Hu, J.; Xu, X.; Ning, N.; Yu, B.; Zhang, L. Multidirectional Triple-Shape-Memory Polymer by Tunable Cross-linking and Crystallization. *ACS Appl. Mater. Interfaces* **2020**, *12* (5), 6426−6435.

(25) Zhang, P.; Wu, B.; Huang, S.; Cai, F.; Wang, G.; Yu, H. UV−vis−NIR Light-Induced Bending of Shape-Memory Polyurethane Composites Doped with Azobenzene and Upconversion Nanoparticles. *Polymer* **2019**, *178*, 121644.

(26) Le, X.; Lu, W.; Zheng, J.; Tong, D.; Zhao, N.; Ma, C.; Xiao, H.; Zhang, J.; Huang, Y.; Chen, T. Stretchable Supramolecular Hydrogels

with Triple Shape Memory Effect. *Chemical Science* **2016**, *7* (11), 6715−6720.
(27) Wu, Y.; Hu, Z.; Huang, H.; Chen, Y. The Design of Triple Shape Memory Polymers with Stable Yet Tunable Temporary Shapes by Introducing Photo-Responsive Units into a Crystalline Domain. *Polym. Chem.* **2019**, *10*, 1537−1543.
(28) Jing, H.; He, L.; Feng, J.; Fu, H.; Guan, S.; Guo, P. High Strength Hydrogels with Multiple Shape Memory Ability Based on Hydrophobic and Electrostatic Interaction. *Soft Matter* **2019**, *15*, 5264−5270.
(29) Liang, R.; Yu, H.; Wang, L.; Amin, B. U.; Wang, N.; Fu, J.; Xing, Y.; Shen, D.; Ni, Z. Triple and Two-Way Reversible Shape Memory Polymer Networks with Body Temperature and Water Responsiveness. *Chem. Mater.* **2021**, *33*, 1190.
(30) Huang, T.; Song, J.; Xing, L.; Li, X.; He, T. Impact of the Ethylene Content on Poly (Ethylene-co-Vinyl Alcohol) Membrane Morphology and Performance via Immersion Precipitation for Lithium Extraction. *J. Membr. Sci.* **2019**, *579*, 172−179.
(31) Bai, Y.; Zhang, J.; Wen, D.; Gong, P.; Liu, J.; Ju, J.; Chen, X. A Reconfigurable, Self-Healing and Near Infrared Light Responsive Thermoset Shape Memory Polymer. *Compos. Sci. Technol.* **2020**, *187*, 107940−107947.
(32) Bai, Y.; Zhang, J.; Wen, D.; Gong, P.; Chen, X. A Poly (Vinyl Butyral)/Graphene Oxide Composite with NIR Light-Induced Shape Memory Effect and Solid-State Plasticity. *Compos. Sci. Technol.* **2019**, *170*, 101−108.
(33) Lotfi Mayan Sofla, R.; Rezaei, M.; Babaie, A.; Nasiri, M. Preparation of Electroactive Shape Memory Polyurethane/Graphene Nanocomposites and Investigation of Relationship between Rheology, Morphology and Electrical Properties. *Composites, Part B* **2019**, *175*, 107090−107100.
(34) Zhao, W.; Liu, L.; Leng, J.; Liu, Y. Thermo-Mechanical Behavior Prediction of Particulate Reinforced Shape Memory Polymer Composite. *Composites, Part B* **2019**, *179*, 107455.
(35) Luzi, F.; Di Michele, A.; Torre, L.; Puglia, D. Active Role of ZnO Nanorods in Thermomechanical and Barrier Performance of Poly(vinyl alcohol-co-ethylene) Formulations for Flexible Packaging. *Polymers* **2019**, *11* (5), 922.
(36) Li, J.; Xie, T. Significant Impact of Thermo-Mechanical Conditions on Polymer Triple-Shape Memory Effect. *Macromolecules* **2011**, *44* (1), 175−180.

https://doi.org/10.1021/acsami.1c05166
ACS Appl. Mater. Interfaces XXXX, XXX, XXX−XXX